Eur. Phys. J. C (2025) 85:1016
https://doi.org/10.1140/epjc/s10052-025-14681-1

THE EUROPEAN PHYSICAL JOURNAL C

Regular Article - Experimental Physics

A unified algorithm for multi-particle correlations between azimuthal angle and transverse momentum in ultra-relativistic nuclear collisions

Emil Gorm Dahlbæk Nielsen, Nina Nathanson, Kristjan Gulbrandsen, You Zhou[a]

Niels Bohr Institute, Jagtvej 155A, 2200 Copenhagen, Denmark

Received: 28 May 2025 / Accepted: 26 August 2025

Abstract Multi-particle correlations between azimuthal angle and mean transverse momentum are a powerful tool for probing size and shape correlations in the initial conditions of ultra-relativistic nuclear collisions. These correlations have also been employed to investigate the structure of the colliding nuclei, including potential nuclear shape phase transitions at the energy frontier. However, the direct implementation of these correlations is highly nontrivial, and prior studies have been mostly limited to lower-order correlations, such as the modified Pearson correlation coefficient, $\rho(v_n^2, [p_T])$. This paper presents a unified framework that employs a recursive algorithm, enabling the efficient evaluation of arbitrary-order correlations while maintaining computational efficiency. This framework is demonstrated using widely adopted transport models, including AMPT and HIJING. The proposed unified algorithm for multi-particle correlations between azimuthal angle and transverse momentum provides a systematic and efficient approach for multi-particle correlation analyses. Its application in experiments at the Relativistic Heavy Ion Collider and the Large Hadron Collider facilitates the exploration of nuclear structure at ultra-relativistic energies.

1 Introduction

Ultrarelativistic collisions of heavy ions at facilities such as RHIC and the LHC create a strongly-coupled, deconfined matter called the Quark-Gluon Plasma (QGP) [1–5]. The collective expansion of the QGP generates anisotropic particle emission patterns due to the geometry of the overlapping region of two colliding nuclei [6]. The anisotropy can be quantified by the anisotropic flow coefficients, v_n, defined as the coefficients of the Fourier expansion of the angular distribution of emitted particles [7]:

$$\frac{dN}{d\varphi} \propto 1 + 2\sum_{n=1}^{\infty} v_n \cos[n(\varphi - \Psi_n)] \tag{1}$$

Anisotropic flow measurements at RHIC and the LHC, together with the systematic comparisons to hydrodynamic model calculations, have shown that the QGP behaves as a near-perfect liquid [8–18], with a shear viscosity over entropy density ratio close to the lowest limit predicted by AdS/CFT theory [19]. Anisotropic flow studies are typically performed via multi-particle azimuthal correlations [20], providing insight into various aspects of QGP dynamics. These flow studies include anisotropic flow coefficients [8–11,13,14,17], event-by-event fluctuations of the flow coefficient [16,21,22], correlations among different flow coefficients [23–26], correlations between different flow symmetry planes [27–31] and flow vector fluctuations/decorrelations [32–37]. Accordingly, anisotropic flow studies are central to understanding the collective properties of the QGP [38–42]. All these multi-particle correlations can be efficiently and precisely measured using the *Generic Framework* [43], or its advanced version, *Generic Algorithm* [44]. A critical aspect of these algorithms is their ability to properly incorporate detector efficiencies, ensuring accurate results for high-order correlations under realistic detector conditions. The v_n coefficients ($n <= 3$) are tightly correlated with the initial eccentricity, ε_n, of the initial state and are, to first-order, a linear hydrodynamic response to the initial state geometry [45]. This sensitivity to initial conditions makes anisotropic flow a valuable probe of the nuclear structure of colliding nuclei [46,47], which is imprinted in the initial geometry due to the low crossing time of the nuclei

[a] e-mail: you.zhou@cern.ch (corresponding author)

Published online: 17 September 2025

compared to collective degrees of freedom, such as rotational and vibrational degrees of freedom [48]. For instance, the relative increase of the measured v_2 in central Xe–Xe collisions compared to central Pb–Pb collisions can only be explained by a sizeable quadrupole deformation, $\beta_2 = 0.207$, of the ^{129}Xe nuclei [49].

Besides the study of anisotropic flow phenomena using multi-particle azimuthal correlations, the mean transverse momentum $[p_T]$ and its fluctuations can also be analysed through multi-particle transverse momentum correlations [50,51]. These correlations provide an alternative approach to probing the initial conditions of heavy-ion collisions. More specifically, the $[p_T]$ fluctuations, resulting from variations in the initial size of the fireball, provide insight into how energy is transferred from the colliding nuclei to the system formed in the early stages of ultra-relativistic nuclear collisions [52]. These fluctuations are strongly correlated with the initial energy density [53]. The $[p_T]$ fluctuations can be estimated by the fluctuations in the initial transverse size, $d_\perp$, of the system via $\delta p_T/[p_T] = \delta d_\perp/d_\perp$ [45,54]. Measurements of the lower orders (mean and variance) of the event-by-event $[p_T]$ fluctuations at RHIC [55–58] and LHC [59–62] and comparison to theoretical models confirm that initial state density fluctuations are necessary to describe the observed $[p_T]$ fluctuations. Measurements of higher-order moments of the $[p_T]$ distribution, such as the skewness and kurtosis [60–62], offer additional insight into the early stages of the ultra-relativistic nuclear collisions by constraining the initial-state fluctuations and even disentangling geometrical and intrinsic sources of fluctuations [63,64]. The $[p_T]$ fluctuations can be studied efficiently to arbitrary order using the generalised multi-particle p_T correlations introduced in [65].

The correlation between v_n^2 and δp_T probes the correlation between the initial size and shape, providing a more comprehensive probe of the initial state. This correlation, in the form of a modified Pearson correlation coefficient, $\rho(v_2^2, \delta p_T)$ [66], has been measured at RHIC [67] and the LHC [68,69]. The $\rho(v_2^2, \delta p_T)$ has the distinct advantage that it is mostly insensitive to final state effects but instead directly reflects the correlations of the initial shape and size [68]. In addition, $\rho(v_2^2, \delta p_T)$ observable show a strong sensitivity to the nucleon width used in initial state models [70] and was used to resolve a conflict in the description of the initial state between competing heavy-ion models [71].

Given the strong connection between v_n-δp_T correlations and the initial-state geometry, these measurements serve as a promising tool for studying nuclear structure at TeV energies. Due to the short crossing time of the colliding nuclei, heavy-ion collisions effectively capture an image of the overlap region between them. In central collisions, where the principal nuclear axes are aligned, this image reflects the ground-state nuclear structure. The anisotropic flow coefficients from two-particle correlations suffice to measure the quadrupole deformation, β_2; however, a nucleus such as ^{129}Xe is expected to exhibit triaxiality, γ, where all three principal axes differ in length. Fully resolving such three-dimensional nuclear structures requires at least a three-particle cumulant. Comparison of measurements of the lowest order v_n-δp_T three-particle correlation, $\rho(v_2^2, \delta p_T)$ to theoretical calculations using the framework of energy-density functional methods [72], has suggested that the ^{129}Xe nuclei are triaxially deformed with a fixed $\gamma = 27°$ [73]. So far, nuclear structure studies in high-energy heavy-ion collisions have assumed rigid structures with fixed parameters of β_2 and γ for ^{129}Xe. However, ^{129}Xe exists within a region of suspected phase transition on the nuclide chart. Within the interacting Boson Model [74] and under the E(5) symmetry group [75,76], the Xenon nuclei undergo a shape phase transition around $^{128\text{-}130}$Xe associated with β-soft and γ-soft deformation [77–81]. Higher-order moments of the joint v_2 and δp_T distribution not only provide further insight into the initial-state properties of heavy-ion collisions but can also be used to explore the nuclear shape phase transition at the TeV energy scales [82].

Traditionally, the lower-order correlation between azimuthal angle and transverse momentum has been measured using the sub-event method to suppress the non-collective contamination. Meanwhile, higher-order cumulants, which involve correlations among multiple particles, are expected to be less biased regarding such non-collective effects. Measuring these cumulants within the entire available phase space significantly increases the statistical precision by utilising the increased number of available particle tuples. This paper presents a unified algorithm to obtain any correlation between arbitrary moments of a set of observables. Recursive formulae to generate the cumulants in specific cases are also presented. The algorithm is showcased through heavy-ion models such as HIJING and AMPT.

2 Unified algorithms for the multi-particle correlations

2.1 One algorithm to rule them all

Two components are involved in computing multi-particle correlations. The first component is the computation of moments of the distribution of various observables. In general, this is $\langle \mathcal{O}_1 \cdot \mathcal{O}_2 \cdots \mathcal{O}_N \rangle$, where $\mathcal{O}_i$ is a specific observable. Care must be taken when computing each observable, as each must be computed from a different particle. Doing so ensures that only dynamical fluctuations are considered and self-correlations are removed. This requirement, when applied naively, drastically increases the necessary computing time. Techniques are then applied to optimize this, but they become progressively more complicated as higher-order moments are investigated. The second compo-

nent is to compute the actual correlation from the moments, $C(\mathcal{O}_1, \mathcal{O}_2, \ldots, \mathcal{O}_N)$. In general, this is done using the cumulant formulation[83]. Cumulants reveal whether a correlation is genuine in that it cannot be reduced to any lower-order set of correlations. Again, the formulae used to compute higher-order correlations become increasingly more complicated to calculate.

To compute multi-particle correlations, $C(\mathcal{O}_1, \mathcal{O}_2, \ldots, \mathcal{O}_N)$, we must first calculate the necessary moments, $M(\mathcal{O}_1, \mathcal{O}_2, \ldots, \mathcal{O}_N)$, defined in Eq. 2.

$$M(\mathcal{O}_1, \cdots, \mathcal{O}_N) = \frac{\sum_{i_1 \neq \cdots \neq i_N} \omega_{1,i_1} \cdots \omega_{N,i_N} \mathcal{O}_{1,i_1} \cdots \mathcal{O}_{N,i_N}}{\sum_{i_1 \neq \cdots \neq i_N} \omega_{1,i_1} \cdots \omega_{N,i_N}}. \quad (2)$$

The requirement that $i_1 \neq \cdots \neq i_N$ creates considerable complication (necessary though to remove self-correlations). One must actually compute $2^N - 1$ different sums of the various observables to remove these self-correlations without manually performing the calculation with nested loops. One must first fill an array (which we will call `S` here) with all the various combinations of observables summed over all particles. This is, for example, $\sum_{i=1}^{N_{particles}} w_{j,i} w_{k,i} w_{l,i} \mathcal{O}_{j,i} \mathcal{O}_{k,i} \mathcal{O}_{l,i}$, if observables j, k, and l are considered. Another array, `SW`, contains only the weights for the denominator. To accomplish this, we use bits to represent whether a variable is or is not included in a sum. So `S[0]=S[1-1]` is $\sum_{i=1}^{N_{particles}} w_{1,i} \mathcal{O}_{1,i}$, because 1 only has the lowest bit on. If we want $\sum_{i=1}^{N_{particles}} w_{1,i} w_{3,i} \mathcal{O}_{1,i} \mathcal{O}_{3,i}$, this is held in S[5-1] as 5 has the binary representation of 101. To fill `S` and `SW`, we use an array N elements long, called `O` here, and fill it with each element being 'weight' × 'observable' for `S` or just 'weight' for `SW`. Then, the following C++ code can be executed for each considered particle in an event to fill `S` and `SW` from those arrays.

```
void fill_array(complex* S,
                complex* O,
                unsigned int n) {

 for (unsigned int i=(1<<n)-1; i>0; --i)
{complex val = 1.; //assign 1
    initially
    for (unsigned int iobs=0; iobs<n;
    ++iobs) {
      if ((i>>iobs)&1) val *= O[iobs];
    }
    S[i-1] += val;
  }
}
```

Note that the `complex` type has to be chosen from whatever is available in someone's code base and could change how initialization works.

Now that `S` and `SW` are filled, two new arrays, also with $2^N - 1$ elements each, called `M` and `MW` are made to hold the moments with all self-correlations removed. The relevant recursion relation used to accomplish this is:

$$\begin{aligned}
&\sum_{i_1 \neq \cdots \neq i_N} A_{1,i_1} \cdots A_{N,i_N} \\
&= \left(\sum_{i_N} A_{N,i_N} \right) \cdot \sum_{i_1 \neq \cdots \neq i_{N-1}} A_{1,i_1} \cdots A_{N-1,i_{N-1}} \\
&\quad - \sum_{i_1 \neq \cdots \neq i_{N-1}} \left(A_{1,i_1} \cdot A_{N,i_1} \right) \cdot A_{2,i_2} \cdots A_{N,i_N} \\
&\quad \vdots \\
&\quad - \sum_{i_1 \neq \cdots \neq i_{N-1}} A_{1,i_1 \cdots N-2,i_{N-2}} \cdot \left(A_{N-1,i_{N-1}} \cdot A_{N,i_{N-1}} \right)
\end{aligned}$$

This recursion relation must be applied many times to produce the algorithm. The following C++ code exploits this relationship in a slightly optimized way to accomplish this. One must run `com_corrs(n,S,M)` and `com_corrs(n,SW,MW)` after filling `S` and `SW` for all particles in the event, where `n` is the number of observables.

```
unsigned int com_fac(unsigned int mask)
   {
  //Compute (n-1)! where n
  // is the number of set bits in mask
  unsigned int fac = 1, bit_count = 0;
  while (mask &= (mask-1)) fac *=
     (++bit_count);
  return fac;
}

complex com_corr(unsigned int mask,
                 complex* S) {
  //Find min val with largest bit set
  unsigned int mask_hold=mask, maskmin
     = 1;
  while (mask_hold >>= 1) maskmin <<= 1;

  complex c = -1*com_fac(mask)*S
    [mask-1];
  for (unsigned int i=(mask-1)&mask;
       i>=maskmin;
       i=(i-1)&mask)
    c -= com_fac(i)*S[i-1]*com_corr((~i)
     &mask, S);
  return c;
}

void com_corrs(unsigned int nobs,
```

```
                complex* S,
                complex* M) {
  for (unsigned int i=(1<<nobs)-1; i>
    0; --i)
    M[i-1] = (i&1?-1:1)*com_corr(i, S);
}
```

Now that `M` and `MW` are filled, the analyser can decide how to average the moments over many events. This can be achieved with unit weighting, multiplicity weighting, or any other weighting method chosen by the analyser. The result averaged separately for each element in the array must end up in some final array (of length $2^N - 1$), which we will call `EM` here. Then, one can use the following code to calculate the cumulant from this by calling `com_cumulant((1«n)-1,EM)` where the first parameter produces a bit mask with all `n` bits on. Note that `(1«n)-1` produces the value $2^N - 1$.

```
complex com_cumulant(unsigned int mask,
           complex* EM,
           unsigned int depth=0) {
  //Find min val with largest bit set
  unsigned int mask_hold = mask,
     maskmin = 1;
  while (mask_hold >>= 1) maskmin <<= 1;

  complex c = 0;
  if ((mask-1)&mask)
    for (unsigned int i=(mask-1)&mask;
         i>=maskmin;
         i=(i-1)&mask)
      c += EM[i-1]*com_cumulant((~i)
                    &mask,
                         EM,
                         depth+1);

  return EM[mask-1]-(depth+1)*c;
}
```

This code is essentially a direct implementation of the following equation from [83], also written in [43]:

$$Cum(\{n\}) = \sum_{l=1}^{n}(l-1)!(-1)^l \sum_{\sum_{i=1}^{l}\{m_i\}=\{n\}} \prod_{i=1}^{l} Mom(\{m_i\})$$

where $\sum_{i-1}^{l}\{m_i\} = \{n\}$ represents all ways to divide $\{n\}$ in l subsets and $Mom(\{m_i\})$ is the moment mentioned in Eq. 2 with the number of elements being m_i.

One can additionally define a new array `C` of length $2^N - 1$ and use the following code to compute the N observable cumulants and all lower order cumulants.

```
void com_cumulants(unsigned int nobs,
                   complex* EM,
                   complex* C) {
  for (unsigned int i=(1<<nobs)-1;
       i>0;
       --i)
    C[i-1] = com_cumulant(i, EM);
}
```

Note, other approaches for the development of higher order cumulants involving multiple observables are also available, please refer to Ref. [84].

2.2 New observables of multi-particle cumulants of azimuthal angle and transverse momentum

Among many different multi-particle correlations between azimuthal angle and transverse momentum, specific multi-particle cumulants of azimuthal angle and transverse momentum (no flow symmetry plane is involved) that we will investigate here are:

$$C(e^{in(\varphi_1-\varphi_2)}, \delta p_{\mathrm{T}}) = C(v_n^2, \delta p_{\mathrm{T}}) = \langle v_n^2 \delta p_{\mathrm{T}}\rangle \tag{3}$$

$$C(e^{in\varphi}, e^{-in\varphi}, \delta p_{\mathrm{T}i}, \delta p_{\mathrm{T}j}) = C(v_n^2, \delta {p_{\mathrm{T}}}^2) = \langle v_n^2 \delta {p_{\mathrm{T}}}^2\rangle - \langle v_n^2\rangle\langle \delta {p_{\mathrm{T}}}^2\rangle \tag{4}$$

$$C(e^{in(\varphi_1-\varphi_2)}, \delta p_{\mathrm{T}i}, \delta p_{\mathrm{T}j}, \delta p_{\mathrm{T}k}) = C(v_n^2, \delta {p_{\mathrm{T}}}^3) = \langle v_n^2 \delta {p_{\mathrm{T}}}^3\rangle - 3\langle v_n^2 \delta p_{\mathrm{T}}\rangle\langle \delta {p_{\mathrm{T}}}^2\rangle - \langle v_n^2\rangle\langle \delta {p_{\mathrm{T}}}^3\rangle \tag{5}$$

$$C(e^{in(\varphi_1+\varphi_2-\varphi_3-\varphi_4)}, \delta p_{\mathrm{T}}) = C(v_n^4, \delta p_{\mathrm{T}}) = \langle v_n^4 \delta p_{\mathrm{T}}\rangle - 4\langle v_n^2 \delta p_{\mathrm{T}}\rangle\langle v_n^2\rangle \tag{6}$$

$$C(e^{in(\varphi_1+\varphi_2-\varphi_3-\varphi_4)}, \delta p_{\mathrm{T}i}, \delta p_{\mathrm{T}j}) = C(v_n^4, \delta {p_{\mathrm{T}}}^2) = \langle v_n^4 \delta {p_{\mathrm{T}}}^2\rangle - 4\langle v_n^2 \delta {p_{\mathrm{T}}}^2\rangle\langle v_n^2\rangle + 4\langle v_n^2\rangle^2\langle \delta {p_{\mathrm{T}}}^2\rangle - 4\langle v_n^2 \delta p_{\mathrm{T}}\rangle^2 - \langle v_n^4\rangle\langle \delta {p_{\mathrm{T}}}^2\rangle \tag{7}$$

All of these can be computed using the generic algorithm presented in this section. One should note that every power of v_n or δp_{T} represents a separate variable that must be computed from individual particles in the same event. Additionally, the notation of v_n^p, where p is some even power, just represents the expected flow coefficient being measured. The actual observable for v_n^2 comes from one observable of $e^{in\phi}$ and another of $e^{-in\phi}$. The cumulants can be normalised by some appropriate choice of denominator [85]. In this paper, the normalisation of $C(v_n^m, \delta {p_{\mathrm{T}}}^k)$ is done by the mth-order anisotropic flow cumulant $c_n\{m\}$ and the p_{T} variance, $\langle \delta {p_{\mathrm{T}}}^2\rangle^{k/2}$. This choice is based on the consideration to normalize the correlator (numinator) by the genuine multi-particle correlations (cumulant) in the mth-order and variance of kth-order p_T correlations. This also allows for avoiding lower-order few-particle correlations

(non-collective effects). Thus, one has

$$NC(v_n^2, \delta p_{\mathrm{T}}) = \frac{C(v_n^2, \delta p_{\mathrm{T}})}{c_n\{2\}\sqrt{\langle \delta {p_{\mathrm{T}}}^2 \rangle}} \tag{8}$$

$$NC(v_n^2, \delta {p_{\mathrm{T}}}^2) = \frac{C(v_n^2, \delta {p_{\mathrm{T}}}^2)}{c_n\{2\}\langle \delta {p_{\mathrm{T}}}^2 \rangle} \tag{9}$$

$$NC(v_n^2, \delta {p_{\mathrm{T}}}^3) = \frac{C(v_n^2, \delta {p_{\mathrm{T}}}^3)}{c_n\{2\}\left(\langle \delta {p_{\mathrm{T}}}^2 \rangle\right)^{3/2}} \tag{10}$$

$$NC(v_n^4, \delta p_{\mathrm{T}}) = \frac{C(v_n^4, \delta p_{\mathrm{T}})}{c_n\{4\}\sqrt{\langle \delta {p_{\mathrm{T}}}^2 \rangle}} \tag{11}$$

$$NC(v_n^4, \delta {p_{\mathrm{T}}}^2) = \frac{C(v_n^4, \delta {p_{\mathrm{T}}}^2)}{c_n\{4\}\langle \delta {p_{\mathrm{T}}}^2 \rangle} \tag{12}$$

3 The models and setup

The a multi-phase transport (AMPT) model [86] is a widely used tool for studying high-energy nuclear collisions; it consists of four key components. The HIJING model [87] simulates the spatial and momentum distributions of mini-jet partons and soft string excitations in the initial conditions. Then, Zhang's parton cascade (ZPC) model [88] simulates the parton cascade, describing parton scatterings based on a screened two-body cross-section. The hadronization occurs through a quark-coalescence particle production mechanism [89], where nearby partons recombine into hadrons. In the end, the hadronic rescatterings are modelled using a relativistic transport (ART) model [90], with the interaction strengths controlled via the time steps. The string melting version of AMPT is used in this paper, where the partonic degree of freedom is enabled. The AMPT-string melting model successfully reproduces particle production and anisotropic flow observed in heavy-ion collisions, which provides valuable inputs for the understanding of the transport properties of QGP [43,91–94]. In addition, it captures the response of final-state collective expansion to the initial state properties (i.e., shape, size and their event-by-event fluctuations), making it a valuable tool for investigating the structure of the nuclei colliding at RHIC and the LHC [65,95–100]. In this paper, the multi-particle correlations (cumulants) between flow coefficients and transverse momentum, $C(v_n^m, \delta {p_{\mathrm{T}}}^k)$, are investigated using AMPT simulations for Pb–Pb and Xe–Xe collisions at the LHC. Notably, calculations of higher-order correlations between azimuthal angle and transverse momentum are presented for the first time. These results can serve as baseline predictions, as they do not account for specific nuclear shapes of ^{208}Pb or ^{129}Xe.

The Heavy Ion Jet INteraction Generator model, HIJING, was developed to study hadron production in high-energy nucleon-nucleon, nucleon-nucleus, and nucleus-nucleus collisions [87]. With additional modifications to the string configuration, this model can also describe bulk hadron spectra and high p_{T} hadron suppression in ultra-relativistic nuclear collisions [101]. At the same time, HIJING has also been used as an initial condition generator for hydrodynamic models [102–104] or parton cascade models like AMPT [86]. However, a key limitation of HIJING is its lack of collective effects, meaning it fails to reproduce the anisotropic flow measurements in ultra-relativistic nuclear collisions at RHIC and the LHC. Because of this, HIJING simulations serve as a baseline study where collective effects are absent, helping to investigate remaining experimental biases originating from non-collective effects [43,44,94,105,106]. This paper employs HIJING simulations to investigate potential biases arising from non-collective effects in the newly proposed multi-particle cumulants of flow coefficients and transverse momentum.

For the AMPT and HIJING model studies on the multi-particle correlations between azimuthal angle and transverse momentum, both the standard and sub-event methods are used. The former one takes the correlated particles from the entire phase space in the pseudorapidity acceptance, such as $0.2 < p_{\mathrm{T}} < 3.0$ GeV/c and $|\eta| < 0.8$, while the latter one takes the azimuthal angle from sub-event A of $-0.8 < \eta^A < -0.4$ and sub-event B of $0.4 < \eta^B < 0.8$, while the particles for the p_{T} correlations are taken from sub-event C of $-0.4 < \eta^C < 0.4$.

4 Results and discussion

It has been established that the higher-order cumulants constructed in this work have the ability to provide unique insights into the structure of colliding nuclei. Their specific sensitivities to the quadrupole deformation β_2 and the triaxiality parameter γ can be predicted by calculating an estimate from the liquid drop model, displayed in Table 1. From this comparison, a statement can be made about the information that is possible to extract from each cumulant.

Generally, the degree of sensitivity that any given cumulant has to β_2 approximately scales with the number of correlated particles used in its calculation. However, the unique combinations of two- and four-particle azimuthal angle correlation components with different orders of δp_{T} across cumulants induce different levels of dependence on γ. Notably, the four-particle cumulant $C(v_2^2, \delta {p_{\mathrm{T}}}^2)$ is completely insensitive to γ in the liquid drop formulation. The six-particle cumulant $C(v_2^4, \delta {p_{\mathrm{T}}}^2)$ has the most significant sensitivity to the γ fluctuations, making it particularly valuable in the context of the potential shape phase transition of the ^{129}Xe nucleus. Due to its increased sensitivity, this cumulant should be sufficient to distinguish between a rigid structure with a fixed triaxiality and the γ fluctuations that would indicate the phase transition.

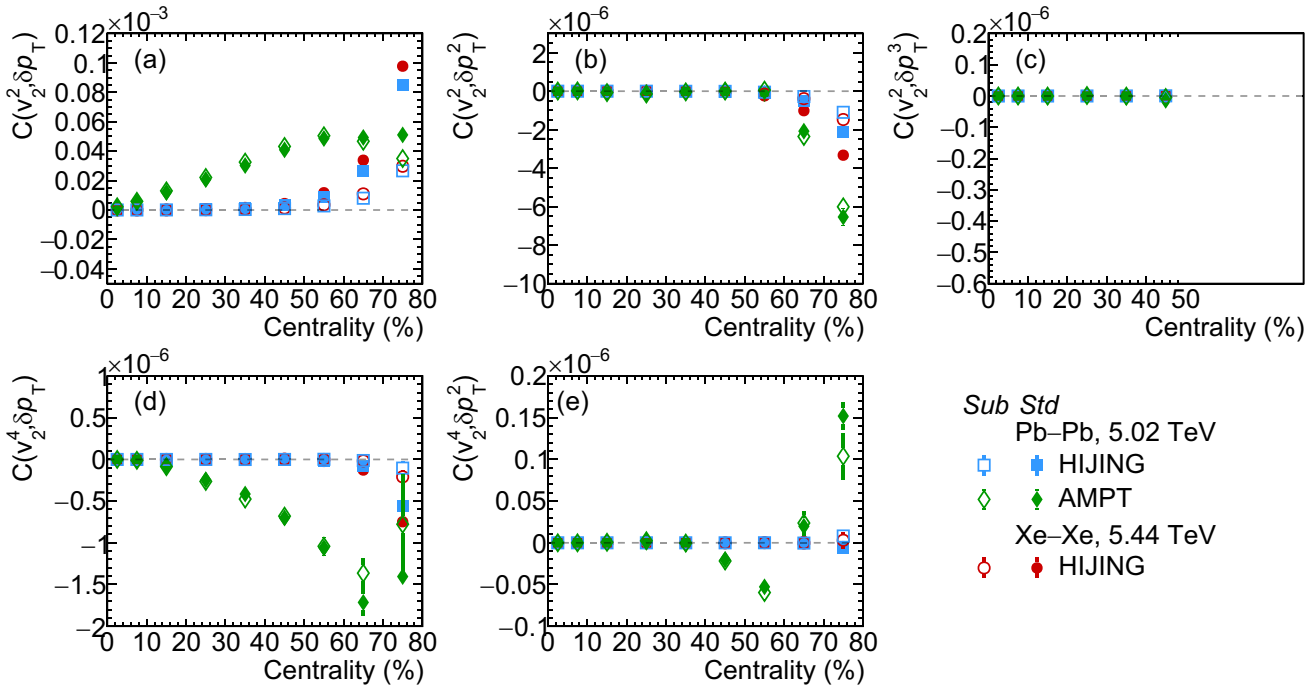

Fig. 1 Centrality dependence of $C(v_n^k, \delta p_T^n)$ in Pb–Pb collisions at 5.02 TeV from AMPT (azure squares) and HIJING (green diamonds) models. Similar calculations in Xe–Xe collisions at 5.44 TeV from HIJING (red circles) are also presented. Calculations from the standard and sub-event methods are shown in solid and open markers, respectively

4.1 Baseline predictions for the collective behaviour

Most of the cumulants derived from the AMPT model have an overall negative trend, with the exception of the three-particle cumulant $C(v_2^2, \delta p_T)$, which shows a positive correlation between v_2^2 and $[p_T]$. For the non-normalized cumulant presented in Fig. 1, $C(v_2^2, \delta p_T)$ in panel (a) appears to have a strong dependence on centrality, increasing linearly before reaching a plateau around a centrality of 60%. This behavior is not reflected in the normalized cumulants (see Fig. 4 in the appendix), which have a relatively weak dependence on centrality. There is, therefore, an indication that this strong centrality dependence is mainly due to the contribution of the two-particle azimuthal angle correlation (or v_n^2) dominating the three-particle cumulant $C(v_2^2, \delta p_T)$. Such a dominant contributions from two-particle azimuthal angle correlation in the centrality dependence $C(v_2^2, \delta p_T)$ is not seen seen in the higher order cumulants $C(v_2^2, \delta {p_T}^2)$ (b) and $C(v_2^2, \delta {p_T}^3)$ (c), where an equal or greater number particles are included in the calculation of the cumulant's transverse momentum component. In these cumulants, very little centrality dependence is observed until the region of 60–80%, where both undergo an exponential increase in magnitude with a negative trend.

For the five-particle cumulant $C(v_2^4, \delta p_T)$, shown in panel (d), the centrality dependence has almost mirrored the trend observed in $C(v_2^2, \delta p_T)$ up to the 60% region, but with a negative correlation. The magnitude is once again attributed to the domination of the four-particle azimuthal angle correlation in the five-particle cumulant. Unlike in the three-particle case, this five-particle cumulant does not go on to reach a plateau but instead reaches a peak between 60 and 70%.

Furthermore, the six-particle cumulant $C(v_2^4, \delta {p_T}^2)$, shown in panel (e), is of special interest due to its aforementioned sensitivity to the γ fluctuations. In the AMPT model, it can be seen that $C(v_2^4, \delta {p_T}^2)$ exhibits a negative trend in mid-central collisions but undergoes a change in sign in the centrality range of 60–70%, and then increases exponentially for more peripheral collisions. There is clearly a strong dependence on centrality in this cumulant.

4.2 Non-collective contamination

As discussed in Sect. 3, the HIJING model provides a baseline study that can be used to assess the contamination of cumulant measurements by non-collective effects, as these are not accounted for within the model. This estimation applies exclusively to experimental measurements and should not be considered a dependable measure of non-collective contamination in the above-discussed AMPT calculations. The HIJING calculations show that all presented

cumulants are consistent with zero in central and mid-central collisions.

In peripheral collisions, non-collective contributions start to present in the HIJING calculations. The magnitude of the contamination varies across the cumulants presented. In cumulants involving correlations of two azimuthal angle observables, a non-zero magnitude is always seen above a centrality of 60–70%, similar to the standard two-particle azimuthal angle correlations.

Conversely, in the six-particle cumulant involving four-particle azimuthal angle correlations, the HIJING baseline is consistent with 0 across the full centrality range in the standard case. This demonstrates the additional suppression of non-collective effects associated with using a higher-order azimuthal angle correlation. It further suggests that the coming measurements of this cumulant will be largely unbiased due to non-collective effects across all centralities. This is particularly beneficial, as it motivates to use of the larger sample accessible through the standard method in the search for potential γ fluctuations using the six-particle cumulant.

Though it has been noted that the HIJING model is most relevant as an estimator of the non-collective contamination in experimental measurements, the presence of this exponential dependence on centrality in the HIJING baseline regions indicates a general contribution from non-collective effects in the peripheral regions, which cannot be entirely disregarded in the AMPT model. These effects are possibly the source of the exponentially increasing trend seen in the peripheral region of the cumulants obtained from the AMPT model.

The cumulants are also presented with and without applying the sub-event method. In the cumulants extracted from HIJING, the method is observed to have the expected effect, consistently reducing the magnitude across the centrality range. However, it must be noted that even when the sub-event method is included, the cumulants $C(v_2^2, \delta p_\mathrm{T})$, $C(v_2^2, \delta {p_\mathrm{T}}^2)$ and $C(v_2^2, \delta {p_\mathrm{T}}^3)$ all maintain their divergence from zero in peripheral collisions. This suggests that the sub-event method is not effective in removing all contributions from non-collective effects within this range of centrality. However, the sub-event method is almost entirely effective at suppressing the non-collective effects in the five-particle cumulant of $C(v_2^4, \delta p_\mathrm{T})$.

5 Summary

In this work, we have developed a *unified algorithm* to study multi-particle correlations between the azimuthal angle and transverse momentum. This algorithm provides a precise and efficient method for computing correlations in any arbitrary order. The technique provides a systematic approach to analysing correlations in complex many-body systems, making it highly relevant for high-energy nuclear physics studies. We introduce several key observables involving multi-particle cumulants of flow coefficients and transverse momentum, denoted as $C(v_n^m, \delta {p_\mathrm{T}}^k)$. Based on the implementation of the *unified algorithm*, these new observables have been validated using the AMPT and HIJING models. The AMPT results, exhibiting characteristic centrality dependence and sign changes, establish a baseline for studying the collective behaviour of these higher-order correlations. Meanwhile, the HIJING results and their deviations from zero serve as an essential reference for understanding non-collective effects in future experimental measurements.

Given the remarkable sensitivity of multi-particle correlations in azimuthal angle and transverse momentum to the initial conditions of heavy-ion collisions, the proposed algorithm emerges as a powerful tool for constraining the uncertainties in the transport properties of the QGP, the key objective of ultra-relativistic nuclear collisions at RHIC and the LHC. Furthermore, by exploiting the close connection between these new correlations and the initial state, the presented algorithm supports the investigation of the structure of the colliding nuclei and enables the exploration of nuclear shape phase transitions in high-energy nuclear collisions, opening new avenues for research at the energy frontier.

Acknowledgements This work is supported by the European Union (ERC, Initial Conditions), VILLUM FONDEN, with grant number 00025462, and Danmarks Frie Forskningsfond (Independent Research Fund Denmark).

Data Availability Statement This manuscript has no associated data. [Authors' comment: Data sharing not applicable to this article as no datasets were generated or analysed during the current study.].

Code Availability Statement Code/software will be made available on reasonable request. [Authors' comment: The code/software generated during and/or analysed during the current study is available from the corresponding author on reasonable request.].

Funded by SCOAP[3].

Appendix A: Additional plots

To verify that the algorithm returns the expected moments, a comparison is performed between a nested loop approach–

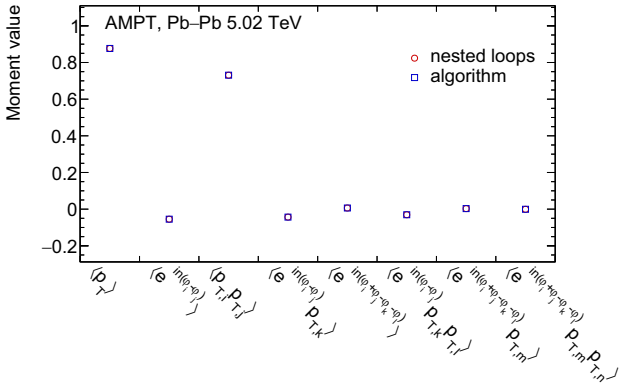

Fig. 2 Comparison of AMPT calculations of all real moments calculated from the observable set $\mathcal{O} = \{e^{in\varphi}, e^{in\varphi}, e^{-in\varphi}, e^{-in\varphi}, p_{\mathrm{T}}, p_{\mathrm{T}}\}$ with six nested loops and with the algorithm presented in this paper. Using the algorithm, the moments correspond to bitsets 010000, 000101, 110000, 010101, 001111, 110101, 011111, 111111

enforcing the $i_1 \neq \cdots \neq i_n$ requirement–and the algorithm under study, using a single event from AMPT. Figure 2 shows the comparison between the nested loop calculations and the algorithm. As expected, the resulting values are identical.

Figure 3 shows the cumulants of flow coefficient and transverse momentum zoomed in on 0–30% centrality. Figure 4 shows the normalized cumulants from Eq. (8)–(12).

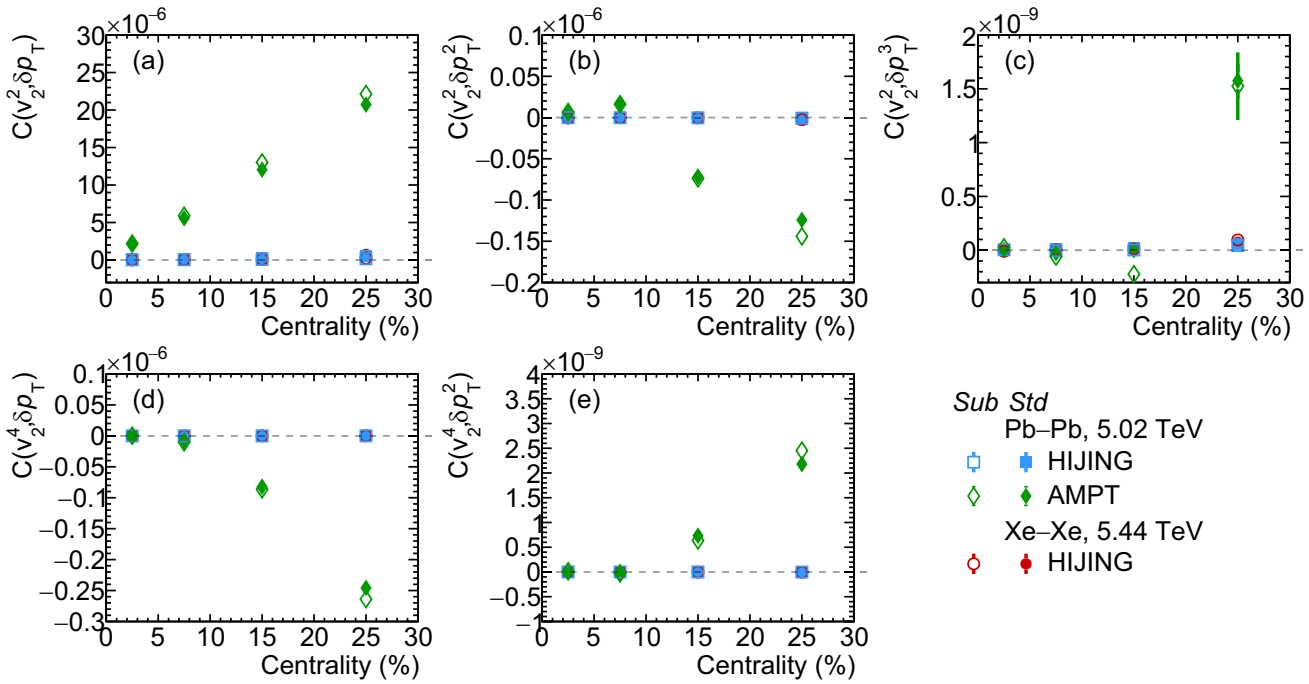

Fig. 3 Centrality dependence of $C(v_n^k, \delta p_{\mathrm{T}}^n)$ in 0–30% central Pb–Pb collisions at 5.02 TeV from AMPT (azure squares) and HIJING (green diamonds) models. Similar calculations in Xe–Xe collisions at 5.44 TeV from HIJING (red circles) are also presented. Calculations from the standard and sub-event methods are shown in solid and open markers, respectively

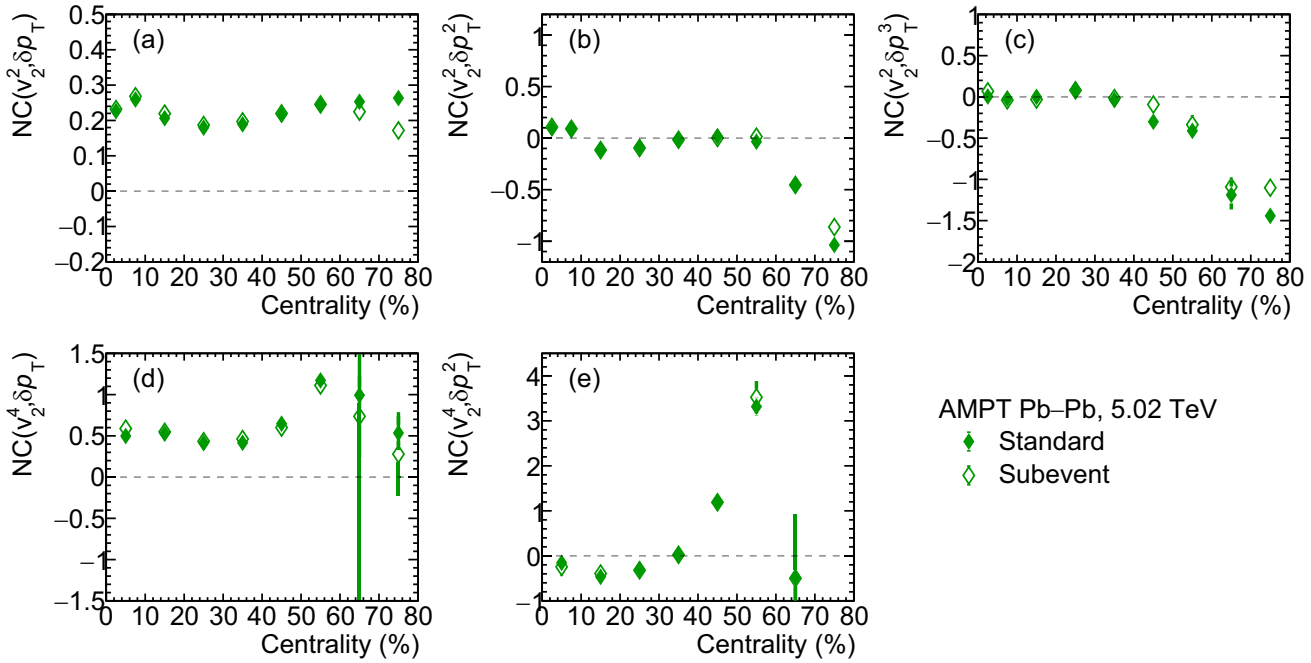

Fig. 4 Centrality dependence of $NC(v_n^k, \delta p_{\mathrm{T}}^n)$ in Pb–Pb collisions at 5.02 TeV from AMPT (azure squares) and HIJING (green diamonds) models. Similar calculations in Xe–Xe collisions at 5.44 TeV from HIJING (red circles) are also presented. Calculations from the standard and sub-event methods are shown in solid and open markers, respectively

Appendix B: Liquid-drop model estimates

The sensitivity of the multi-particle cumulants of flow coefficient and transverse momentum can be estimated by the liquid drop model [107]. These estimates are shown for the observables presented in this paper in Table 1.

Table 1 Selected multi-particle cumulants of flow coefficients and transverse momentum in a liquid-drop model potential averaged over random orientations

Final state cumulant	Initial state cumulant	Liquid-drop model
$C(v_2^2, \delta p_{\mathrm{T}})$	$\left\langle \varepsilon_2^2 \frac{\delta d_\perp}{d_\perp} \right\rangle$	$-\frac{3\sqrt{5}\cos(3\gamma)\langle\beta_2^3\rangle}{28\pi^{3/2}}$
$C(v_2^2, \delta p_{\mathrm{T}}{}^2)$	$\left\langle \varepsilon_2^2 \left(\frac{\delta d_\perp}{d_\perp}\right)^2 \right\rangle - \langle\varepsilon_2^2\rangle \left\langle \left(\frac{\delta d_\perp}{d_\perp}\right)^2 \right\rangle$	$\frac{3\left(5\langle\beta_2^4\rangle - 7\langle\beta_2^2\rangle^2\right)}{224\pi^4}$
$C(v_2^2, \delta p_{\mathrm{T}}{}^3)$	$\left\langle \varepsilon_2^2 \left(\frac{\delta d_\perp}{d_\perp}\right)^3 \right\rangle - \langle\varepsilon_2^2\rangle \left\langle \left(\frac{\delta d_\perp}{d_\perp}\right)^3 \right\rangle - 3\left\langle \varepsilon_2^2 \frac{\delta d_\perp}{d_\perp} \right\rangle \left\langle \left(\frac{\delta d_\perp}{d_\perp}\right)^2 \right\rangle$	$\frac{3\sqrt{5}\cos(3\gamma)\left(11\langle\beta_2^2\rangle\langle\beta_2^3\rangle - 5\langle\beta_2^5\rangle\right)}{2464\pi^{5/2}}$
$C(v_2^4, \delta p_{\mathrm{T}})$	$\left\langle \varepsilon_2^4 \frac{\delta d_\perp}{d_\perp} \right\rangle - 4\langle\varepsilon_2^2\rangle \left\langle \varepsilon_2^2 \frac{\delta d_\perp}{d_\perp} \right\rangle$	$\frac{9\sqrt{5}\cos(3\gamma)\left(11\langle\beta_2^2\rangle\langle\beta_2\rangle^3 - 5\beta_2^5\right)}{154\pi^{5/2}}$
$C(v_2^4, \delta p_{\mathrm{T}}{}^2)$	$\left\langle \varepsilon_2^4 \left(\frac{\delta d_\perp}{d_\perp}\right)^2 \right\rangle - \langle\varepsilon_2^4\rangle \left\langle \left(\frac{\delta d_\perp}{d_\perp}\right)^2 \right\rangle - 4\langle\varepsilon_2^2\rangle \left\langle \varepsilon_2^2 \left(\frac{\delta d_\perp}{d_\perp}\right)^2 \right\rangle - 4\left\langle \varepsilon_2^2 \frac{\delta d_\perp}{d_\perp} \right\rangle^2 + 4\langle\varepsilon_2^2\rangle^2 \left\langle \left(\frac{\delta d_\perp}{d_\perp}\right)^2 \right\rangle$	$\frac{3\left(42042\langle\beta_2^2\rangle^3 - 17160\cos(3\gamma)\langle\beta_2^3\rangle^2 - 45045\langle\beta_2^2\rangle\langle\beta_2^4\rangle + 175(53+16\cos(6\gamma))\langle\beta_2^6\rangle\right)}{32032\pi^6}$

References

1. I. Arsene et al. (BRAHMS), Nucl. Phys. A **757**, 1 (2005). arXiv:nucl-ex/0410020
2. J. Adams et al. (STAR), Nucl. Phys. A **757**, 102 (2005). arXiv:nucl-ex/0501009
3. K. Adcox et al. (PHENIX), Nucl. Phys. A **757**, 184 (2005). arXiv:nucl-ex/0410003
4. B.B. Back et al. (PHOBOS), Nucl. Phys. A **757**, 28 (2005). arXiv:nucl-ex/0410022
5. S. Acharya et al. (ALICE), Eur. Phys. J. C **84**, 813 (2024). arXiv:2211.04384
6. J.-Y. Ollitrault, Phys. Rev. D **46**, 229 (1992)
7. S. Voloshin, Y. Zhang, Z. Phys. C **70**, 665 (1996). arXiv:hep-ph/9407282
8. K.H. Ackermann et al. (STAR), Phys. Rev. Lett. **86**, 402 (2001). arXiv:nucl-ex/0009011
9. S.S. Adler et al. (PHENIX), Phys. Rev. Lett. **91**, 182301 (2003). arXiv:nucl-ex/0305013
10. K. Aamodt et al. (ALICE), Phys. Rev. Lett. **105**, 252302 (2010). arXiv:1011.3914
11. K. Aamodt et al. (ALICE), Phys. Rev. Lett. **107**, 032301 (2011). arXiv:1105.3865
12. B.B. Abelev et al. (ALICE), JHEP **06**, 190 (2015). arXiv:1405.4632
13. J. Adam et al. (ALICE), Phys. Rev. Lett. **116**, 132302 (2016). arXiv:1602.01119
14. G. Aad et al. (ATLAS), Phys. Rev. C **86**, 014907 (2012). arXiv:1203.3087
15. G. Aad et al. (ATLAS), Phys. Lett. B **707**, 330 (2012). arXiv:1108.6018
16. G. Aad et al., ATLAS. JHEP **11**, 183 (2013). arXiv:1305.2942
17. S. Chatrchyan et al. (CMS), Eur. Phys. J. C **72**, 2012 (2012). arXiv:1201.3158
18. S. Chatrchyan et al. (CMS), Phys. Rev. C **87**, 014902 (2013). arXiv:1204.1409
19. P. Kovtun, D.T. Son, A.O. Starinets, Phys. Rev. Lett. **94**, 111601 (2005). arXiv:hep-th/0405231
20. N. Borghini, P.M. Dinh, J.-Y. Ollitrault, Phys. Rev. C **63**, 054906 (2001). arXiv:nucl-th/0007063
21. A.M. Sirunyan et al. (CMS), Phys. Lett. B **789**, 643 (2019). arXiv:1711.05594
22. S. Acharya et al. (ALICE), JHEP **07**, 103 (2018). arXiv:1804.02944
23. G. Aad et al. (ATLAS), Phys. Rev. C **92**, 034903 (2015). arXiv:1504.01289
24. J. Adam et al. (ALICE), Phys. Rev. Lett. **117**, 182301 (2016). arXiv:1604.07663
25. S. Acharya et al. (ALICE), Phys. Lett. B **818**, 136354 (2021). arXiv:2102.12180
26. J. Adam et al. (STAR), Phys. Lett. B **783**, 459 (2018). arXiv:1803.03876
27. G. Aad et al. (ATLAS), Phys. Rev. C **90**, 024905 (2014). arXiv:1403.0489
28. S. Acharya et al. (ALICE), Phys. Lett. B **773**, 68 (2017). arXiv:1705.04377
29. S. Acharya et al. (ALICE), JHEP **06**, 147 (2020). arXiv:1912.00740
30. S. Acharya et al. (ALICE), JHEP **05**, 085 (2020). arXiv:2002.00633
31. A.M. Sirunyan et al. (CMS), Eur. Phys. J. C **80**, 534 (2020). arXiv:1910.08789
32. S. Chatrchyan et al. (CMS), JHEP **02**, 088 (2014). arXiv:1312.1845
33. A.M. Sirunyan et al. (CMS), Phys. Rev. C **96**, 064902 (2017). arXiv:1708.07113
34. S. Acharya et al. (ALICE), JHEP **09**, 032 (2017). arXiv:1707.05690
35. S. Acharya et al. (ALICE), Phys. Rev. C **107**, L051901 (2023). arXiv:2206.04574
36. S. Acharya et al. (ALICE), Phys. Rev. C **109**, 065202 (2024). arXiv:2403.15213
37. G. Aad et al. (ATLAS), (2023). arXiv:2308.16745
38. S.A. Voloshin, A.M. Poskanzer, R. Snellings, Landolt-Bornstein **23**, 293 (2010). arXiv:0809.2949
39. U. Heinz, R. Snellings, Ann. Rev. Nucl. Part. Sci. **63**, 123 (2013). arXiv:1301.2826
40. E. Shuryak, Rev. Mod. Phys. **89**, 035001 (2017). arXiv:1412.8393
41. H. Song, Y. Zhou, K. Gajdosova, Nucl. Sci. Tech. **28**, 99 (2017). arXiv:1703.00670
42. W. Busza, K. Rajagopal, W. van der Schee, Ann. Rev. Nucl. Part. Sci. **68**, 339 (2018). arXiv:1802.04801
43. A. Bilandzic, C.H. Christensen, K. Gulbrandsen, A. Hansen, Y. Zhou, Phys. Rev. C **89**, 064904 (2014). arXiv:1312.3572
44. Z. Moravcova, K. Gulbrandsen, Y. Zhou, Phys. Rev. C **103**, 024913 (2021). arXiv:2005.07974
45. H. Niemi, K.J. Eskola, R. Paatelainen, Phys. Rev. C **93**, 024907 (2016). arXiv:1505.02677
46. J. Jia et al., Nucl. Sci. Tech. **35**, 220 (2024). arXiv:2209.11042
47. A. Dimri, S. Bhatta, J. Jia, Eur. Phys. J. A **59**, 45 (2023). arXiv:2301.03556
48. J. Jia, (2025). arXiv:2501.16071
49. S. Acharya et al. (ALICE), (2024). arXiv:2409.04343
50. W. Broniowski, M. Chojnacki, L. Obara, Phys. Rev. C **80**, 051902 (2009). arXiv:0907.3216
51. P. Bozek, W. Broniowski, Phys. Rev. C **85**, 044910 (2012). arXiv:1203.1810
52. G. Giacalone, F.G. Gardim, J. Noronha-Hostler, J.-Y. Ollitrault, Phys. Rev. C **103**, 024910 (2021). arXiv:2004.09799
53. G. Giacalone, F.G. Gardim, J. Noronha-Hostler, J.-Y. Ollitrault, Phys. Rev. C **103**, 024909 (2021). arXiv:2004.01765
54. B. Schenke, C. Shen, D. Teaney, Phys. Rev. C **102**, 034905 (2020). arXiv:2004.00690
55. J. Adams et al. (STAR), Phys. Rev. C **72**, 044902 (2005). arXiv:nucl-ex/0504031
56. K. Adcox et al. (PHENIX), Phys. Rev. C **66**, 024901 (2002). arXiv:nucl-ex/0203015
57. S.S. Adler et al., PHENIX. Phys. Rev. Lett. **93**, 092301 (2004). arXiv:nucl-ex/0310005
58. J. Adams et al. (STAR), Phys. Rev. C **71**, 064906 (2005). arXiv:nucl-ex/0308033
59. B.B. Abelev et al. (ALICE), Eur. Phys. J. C **74**, 3077 (2014). arXiv:1407.5530
60. S. Acharya et al. (ALICE), Phys. Lett. B **850**, 138541 (2024). arXiv:2308.16217
61. G. Aad et al. (ATLAS), Phys. Rev. Lett. **133**, 252301 (2024). arXiv:2407.06413
62. I.J. Abualrob et al. (ALICE), (2025). arXiv:2506.10394
63. R. Samanta, S. Bhatta, J. Jia, M. Luzum, J.-Y. Ollitrault, Phys. Rev. C **109**, L051902 (2024). arXiv:2303.15323
64. R. Samanta, J.a.P. Picchetti, M. Luzum, J.-Y. Ollitrault, Phys. Rev. C **108**, 024908 (2023). arXiv:2306.09294
65. E.G.D. Nielsen, F.K. Rømer, K. Gulbrandsen, Y. Zhou, Eur. Phys. J. A **60**, 38 (2024). arXiv:2312.00492
66. P. Bozek, Phys. Rev. C **93**, 044908 (2016). arXiv:1601.04513
67. M.I. Abdulhamid et al. (STAR), Nature **635**, 67 (2024). arXiv:2401.06625
68. S. Acharya et al. (ALICE), Phys. Lett. B **834**, 137393 (2022). arXiv:2111.06106

69. G. Aad et al. (ATLAS), Phys. Rev. C **107**, 054910 (2023). arXiv:2205.00039
70. G. Giacalone, B. Schenke, C. Shen, Phys. Rev. Lett. **128**, 042301 (2022). arXiv:2111.02908
71. G. Nijs, W. van der Schee, Phys. Rev. Lett. **129**, 232301 (2022). arXiv:2206.13522
72. M. Bender, P.-H. Heenen, P.-G. Reinhard, Rev. Mod. Phys. **75**, 121 (2003)
73. B. Bally, M. Bender, G. Giacalone, V. Somà, Phys. Rev. Lett. **128**, 082301 (2022). arXiv:2108.09578
74. F. Iachello, A. Arima, *The Interacting Boson Model, Cambridge Monographs on Mathematical Physics* (Cambridge University Press, Cambridge, 1987)
75. F. Iachello, Phys. Rev. Lett. **87**, 052502 (2001)
76. F. Iachello, Phys. Rev. Lett. **85**, 3580 (2000)
77. Z.P. Li, T. Niksic, D. Vretenar, J. Meng, Phys. Rev. C **81**, 034316 (2010). arXiv:1003.4109
78. R. Rodriguez-Guzman, P. Sarriguren, Phys. Rev. C **76**, 064303 (2007). arXiv:0711.1308
79. R. Fossion, D. Bonatsos, G.A. Lalazissis, Phys. Rev. C **73**, 044310 (2006). arXiv:nucl-th/0603024
80. K. Nomura, T. Nikšić, D. Vretenar, Phys. Rev. C **96**, 014304 (2017). arXiv:1704.07101
81. L.M. Robledo, R.R. Rodriguez-Guzman, P. Sarriguren, Phys. Rev. C **78**, 034314 (2008)
82. S. Zhao, H.-J. Xu, Y. Zhou, Y.-X. Liu, H. Song, Phys. Rev. Lett. **133**, 192301 (2024). arXiv:2403.07441
83. R. Kubo, J. Phys. Soc. **17**, 1100 (1962)
84. C. Pruneau, V. Gonzalez, A. Marin, S. Basu, Phys. Rev. C **109**, 044904 (2024). arXiv:2310.07618
85. P. Bozek, R. Samanta, Phys. Rev. C **104**, 014905 (2021). arXiv:2103.15338
86. Z.-W. Lin, C.M. Ko, B.-A. Li, B. Zhang, S. Pal, Phys. Rev. C **72**, 064901 (2005). arXiv:nucl-th/0411110
87. X.-N. Wang, M. Gyulassy, Phys. Rev. Lett. **86**, 3496 (2001). arXiv:nucl-th/0008014
88. B. Zhang, Comput. Phys. Commun. **109**, 193 (1998). arXiv:nucl-th/9709009
89. L.-W. Chen, C.M. Ko, Phys. Lett. B **634**, 205 (2006). arXiv:nucl-th/0505044
90. B.-A. Li, C.M. Ko, Phys. Rev. C **52**, 2037 (1995). arXiv:nucl-th/9505016
91. B.H. Alver, C. Gombeaud, M. Luzum, J.-Y. Ollitrault, Phys. Rev. C **82**, 034913 (2010). arXiv:1007.5469
92. J. Xu, C.M. Ko, Phys. Rev. C **84**, 014903 (2011). arXiv:1103.5187
93. Y. Zhou, K. Xiao, Z. Feng, F. Liu, R. Snellings, Phys. Rev. C **93**, 034909 (2016). arXiv:1508.03306
94. E.G. Nielsen, Y. Zhou, Eur. Phys. J. C **83**, 545 (2023). arXiv:2211.13651
95. G. Giacalone, J. Jia, C. Zhang, Phys. Rev. Lett. **127**, 242301 (2021). arXiv:2105.01638
96. C. Zhang, J. Jia, Phys. Rev. Lett. **128**, 022301 (2022). arXiv:2109.01631
97. J. Jia, G. Giacalone, C. Zhang, Phys. Rev. Lett. **131**, 022301 (2023). arXiv:2206.10449
98. Z. Lu, M. Zhao, X. Li, J. Jia, Y. Zhou, Eur. Phys. J. A **59**, 279 (2023). arXiv:2309.09663
99. X.-L. Zhao, G.-L. Ma, Y. Zhou, Z.-W. Lin, C. Zhang, (2024). arXiv:2404.09780
100. C. Zhang, J. Chen, G. Giacalone, S. Huang, J. Jia, Y.-G. Ma, (2024). arXiv:2404.08385
101. W.-T. Deng, X.-N. Wang, R. Xu, Phys. Rev. C **83**, 014915 (2011). arXiv:1008.1841
102. X. Zhu, Y. Zhou, H. Xu, H. Song, Phys. Rev. C **95**, 044902 (2017). arXiv:1608.05305
103. W. Zhao, H.-J. Xu, H. Song, Eur. Phys. J. C **77**, 645 (2017). arXiv:1703.10792
104. W. Zhao, Y. Zhou, K. Murase, H. Song, Eur. Phys. J. C **80**, 846 (2020). arXiv:2001.06742
105. P. Huo, K. Gajdošová, J. Jia, Y. Zhou, Phys. Lett. B **777**, 201 (2018). arXiv:1710.07567
106. S. Bhatta, C. Zhang, J. Jia, Phys. Rev. C **105**, 024904 (2022). arXiv:2112.03397
107. J. Jia, Phys. Rev. C **105**, 044905 (2022). arXiv:2109.00604